

# Slim, Sparse, and Shortcut Networks

Fenglei Fan<sup>1</sup>, Dayang Wang<sup>2</sup>, Hengtao Guo<sup>1</sup>, Qikui Zhu<sup>1</sup>, Pingkun Yan<sup>1\*</sup>, Ge Wang<sup>1\*</sup> and Hengyong Yu<sup>2\*</sup>

**Abstract**—Over the recent years, deep learning has become the mainstream data-driven approach to solve many real-world problems in many important areas. Among the successful network architectures, shortcut connections are well established to take the outputs of earlier layers as additional inputs to later layers, which have produced excellent results. Despite the extraordinary power, there remain important questions on the underlying mechanism and associated functionalities regarding shortcuts. For example, why are the shortcuts powerful? How to tune the shortcut topology to optimize the efficiency and capacity of the network model? Along this direction, here we first demonstrate a topology of shortcut connections that can make a one-neuron-wide deep network approximate any univariate function. Then, we present a novel width-bounded universal approximator in contrast to depth-bounded universal approximators. Next we demonstrate a family of theoretically equivalent networks, corroborated by the concerning statistical significance experiments, and their graph spectral characterization, thereby associating the representation ability of neural network with their graph spectral properties. Furthermore, we shed light on the effect of concatenation shortcuts on the margin-based multi-class generalization bound of deep networks. Encouraged by the positive results from the bounds analysis, we instantiate a slim, sparse, and shortcut network (S3-Net) and the experimental results demonstrate that the S3-Net can achieve better learning performance than the densely connected networks and other state-of-the-art models on some well-known benchmarks.

## I. INTRODUCTION

Recently, deep learning [1], [2] has been rapidly evolving, and achieved great successes in many applications [3], [4], [5], [6], [7], [8]. Since the AlexNet was reported [9], more and more state-of-the-art models were developed; for example, Inception [10], Network in Network [11], VGG [12], ResNet [13], DenseNet [14] and so on. These advanced models play an important role of backbone architecture, pushing the boundaries of deep learning on the downstream tasks. Among them, it is noted that there were great efforts made to explore the use of skip connections based on neural architecture search (NAS) or heuristics [15], [16], [17], [18], [19], [20]. For example, shortcut topology was searched based on the framework of a lightweight network for super-resolution tasks in [15]. Hypercolumn network [16] stacked the units at all layers as concatenated feature descriptors to

obtain semantic information and precise localization. Highway Network [19] achieved great successes in training very deep networks. Fractal Network [20] used a different skip connection design strategy, by which interacting sub-paths were used without any pass-through or residual connections.

In the 90s, a so-called universal approximation theorem was proved to justify the representation power of a network. Given a sufficient number of neurons, which means the network is extremely wide, a one-hidden-layer network can express any continuous function [21], [22]. In recent years, inspired by successes of deep learning, intensive efforts were put to justify the advantages of depth over width of networks. The basic idea behind these results is to construct a special class of functions that a deep network can sufficiently represent but shallow networks cannot [23], [24], [25], [26], [27], [28]. However, it is tricky that despite the incorporation of shortcuts greatly promotes the success of deep learning in solving the real-world problems, the theoretical works are few to explain the representation ability and generalization ability of shortcuts. Motivated by the successes of ResNet, DenseNet and exemplary models with shortcuts, in this paper we present our findings on the power of shortcuts in a novel by-pass connection architecture.

Specifically, we investigate a novel shortcut topology: Slim, Sparse, and Shortcut Network (S3-Net), wherein shortcuts are used to bridge all the previous layers and the final layers in the whole network or a block (see Figure 1). Although it has been not thoroughly investigated, such a network structure has demonstrated effectiveness as a backbone network in CT image denoising and super-resolution [46], [47]. Here, we study the expressive power and generalization ability of this network structure theoretically and experimentally, by which the insights are extracted onto the utility of shortcuts for a network.

First, we show that the one-neuron-wide S3-Net can approximate any univariate function, thereby theoretically casting light on the power of shortcuts. Simply speaking, adding shortcuts can lead to a more compact network structure. Furthermore, we report an alternative novel width-bounded universal approximator by using Kolmogorov-Arnold representation theorem [29], in contrast to the depth-bounded universal approximator [30], [31], [32]. Given the input of  $d$  dimensions, the required width is no more than  $2d^2 + d$  in our scheme. Then, we present a family of theoretically equivalent networks, corroborated by the concerning statistical significance experiments, and their graph spectral characterization, thereby associating the representation ability of neural network with their graph spectral properties. Next, we analyze the effect of concatenation shortcuts on

\*Drs. Pingkun Yan, Ge Wang and Hengyong Yu serve as co-corresponding authors. This work was partially supported by IBM AI Horizon Scholarship.

<sup>1</sup>Fenglei Fan (fanf2@rpi.edu), Hengtao Guo, Qikui Zhu, Pingkun Yan and Ge Wang (wangg6@rpi.edu) are with Department of Biomedical Engineering, Rensselaer Polytechnic Institute, Troy, NY 12180, USA

<sup>2</sup>Dayang Wang and Hengyong Yu (hengyong\_yu@uml.edu) are with Department of Electrical and Computer Engineering, University of Massachusetts, Lowell, MA 01854, USA

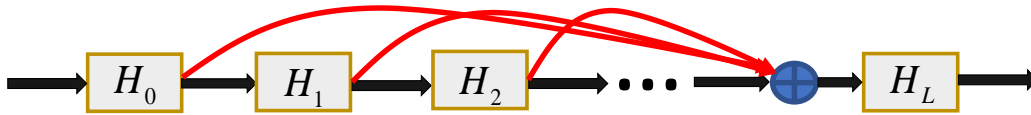


Fig. 1. Topology of our proposed S3-Net. There are two aggregation approaches; residual connection and concatenation. In the following, we denote summation and concatenation as  $+$  and  $\oplus$  respectively.

the generalization bound of deep networks and show that S3-Net enjoys a tighter generalization bound compared with that of DenseNet. Encouraged by the positive results from the bound analysis, we instantiate the S3-Net in the form of both concatenation connections on some well-known classification benchmarks. The experimental results demonstrate that S3-Net can achieve better learning performance than the densely connected networks and other state-of-the-art models.

To put our contributions in perspective, we would like to review the existing results in the literature in three aspects. 1) It was reported in [32] that with the use of residual connections, one neuron is sufficient for the ResNet to approximate any Lebesgue-integrable function. In [33], it was showcased that the residual networks demonstrate ensemble-like behaviour. Liu *et al.* [48] studied the convergence behavior of a two-layer network and proved that the optimization of a two-layer ResNet can avoid spurious minima under mild restrictions. Bartlett *et al.* [36] studied a spectrally-normalized margin bound to discuss the influence of residual connections on the generalization ability of deep networks. It was shown that the margin-based multi-class generalization bound of ResNet is of the same magnitude as that of chain-like counterparts. Unfortunately, the literature is few pertaining to justifying the power of shortcuts in deep learning. Here, we not only justify the representation ability of shortcuts by showing that the incorporation of shortcuts in the form of the S3-Net topology can facilitate extremely narrow networks, but also conduct the generalization bound analysis of DenseNet and S3-Net from three different theories.

2) The work closely related to ours was done by [35], who heuristically proposed a variant of a sparsified DenseNet and numerically demonstrated that the sparsified network is efficient and robust as compared to the ResNet and DenseNet. However, their study was not theoretical and did not answer why such a structure can outperform the ResNet and DenseNet. In contrast, here we approach the shortcut design through mathematical analysis, which is distinct from the heuristic approaches as well as computationally expensive NAS methods. The vehicle admitted by mathematical analysis is with the advantages of theoretical accountability.

3) As far as the universal approximation is concerned, to realize a strong representation power, the network was previously made as wide as needed. Impressively, in Lu *et al.* [30], giving at most  $d+4$  neurons per layer and allowing an infinite depth, a fully-connected deep network with the ReLU activation can approximate a Lebesgue-integrable  $d$ -dimension function accurately in the  $L^1$ -norm sense. As a straightforward extension, Lin *et al.* [32] compressed  $d+4$

into 1 by using residual connections, which used similar mathematical techniques in [30]. Along this direction, we present a novel width-limited universal approximator with width that is no more than  $2d^2 + d$ . Although the width bound in our universal approximator is larger than those set by Lu *et al.* and Lin *et al.*, our work is still valuable because of the scarcity of width-bounded universal approximators.

In summary, our contributions are three-fold: 1) We show the efficacy admitted by the shortcut connections with constructive analysis that a one-neuron-per-layer network can approximate a general univariate function. Concurrent with the theorem in Lin *et al.*, we mathematically justify that shortcut connections are powerful in making a compact structure. And then we report a width-limited universal approximator, which is made possible by the employment of shortcuts in light of Kolmogorov-Arnold representation theorem. 2) We present a family of theoretically equivalent networks, followed by the statistical significance experiments, and their graph spectral characterization. 3) We explore the impact of concatenation shortcuts on the generalization bound of deep networks from three different theories and reveal that several generalization bounds of S3-Net are tighter than those of DenseNet. We instantiate the S3-Net and obtain experimental results on the CIFAR-100 to show that the S3-Net achieves better classification performance than DenseNet and other state-of-the-art models, which agrees with the bounds analysis.

## II. ONE-NEURON-WIDE S3-NET

For an extremely slim network with only one neuron in every layer, adding shortcuts shown in Figure 1, can make the network approximate any univariate function in the sense of the  $L^\infty$  distance. We focus on the S3-Net topology in Figure 1. Then, mathematically we first make the following conjecture:

**Conjecture 1:** With the ReLU activation, for any continuous function  $g : [0, 1] \rightarrow \mathbb{R}$  and any given precision  $\delta > 0$ , there exists a neural network  $G$  of S3-Net topology and one neuron in each layer such that

$$\sup_{x \in [0, 1]} |g(x) - G(x)| < \delta \quad (1)$$

**The sketch of our constructive analysis:** We show how to use a one-neuron S3-Net to approximate a continuous piecewise linear function. Mathematically, any univariate continuous function can be approximated by a continuous piecewise linear function within any given closeness. Therefore, the key becomes how to implement this piecewise approximation by a one-neuron-wide S3-Net structure. In

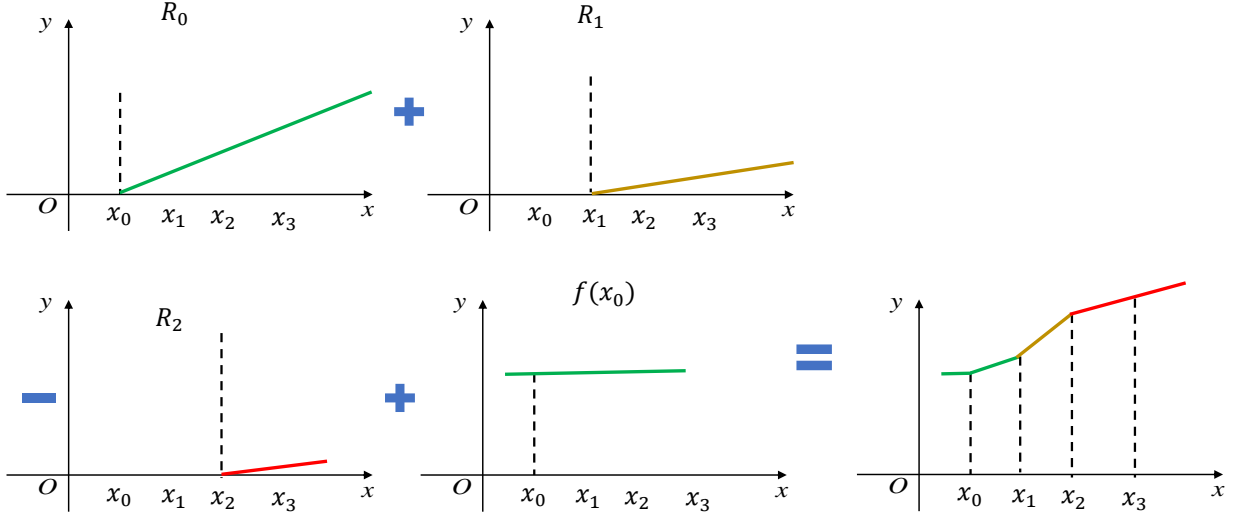


Fig. 2. An example of  $\sum_{i=0}^{L-1} \text{sgn}(i)R_i + f(x_0)$  as  $R_0 + R_1 - R_2 + f(x_0)$  to illustrate how S3-Net represent  $f(x)$ .

our scheme, we use the ReLU as the activation functions for all the neurons except the output neuron. By convention of regression tasks, the activation function of the output layer is linear. Our construction is to make each neuron represent a piecewise function and then we use shortcuts to aggregate these piecewise linear segments over the interval of interest in the output neuron.

**Preliminaries:** According to the spline fitting theory, any continuous function  $g(x)$  can be approximated by a piecewise linear function  $f(x)$  at any accuracy in the  $L^\infty$  sense. Here, without loss of generality, we assume that  $f(x)$  is continuous and the first piece of  $f(x)$  is monotonically decreasing or increasing. Then, when the interval  $[0, 1]$  is partitioned into very tiny sub-intervals, a general function can be well approximated by a continuous piecewise function  $f(x)$  with  $L$  segments, where the first segment is non-constant. Therefore, to demonstrate the correctness of Conjecture 1, we just need to use a one-neuron-wide S3-Net to implement  $f(x)$ . Here, we show an explicit expression of  $f(x)$  as follows:

$$f(x) = \begin{cases} f_0(x) & x \in [x_0, x_1] \\ f_1(x) & x \in (x_1, x_2] \\ f_2(x) & x \in (x_2, x_3] \\ \vdots & \\ f_{L-1}(x) & x \in (x_{L-1}, x_L] \end{cases} \quad (2)$$

where

$$f_i(x) = \begin{cases} \frac{f(x_{i+1})-f(x_i)}{x_{i+1}-x_i}(x-x_i) + f(x_i) & x \in [x_i, x_{i+1}] \\ 0 & x \notin [x_i, x_{i+1}]. \end{cases} \quad (3)$$

Specially,  $x_0 = 0$ ,  $x_L = 1$ ,  $f_0, f_1, \dots, f_{L-1}$  satisfy that  $f_i(x_{i+1}) = f_{i+1}(x_{i+1})$  and  $f(x_0) \neq f(x_1)$ , which jointly reflect continuity and monotonicity imposed on  $f(x)$ . In addition, please note that by default neighboring segments

should have different slopes, otherwise they will be combined as one segment.

**Analysis:** Now, let us show how to select parameters of a one-neuron-wide S3-Net to express  $f(x)$ . The outputs of neurons are respectively denoted as  $R_0, R_1, R_2, \dots, R_{L-1}$ . Without loss of generality, we assume a bounded function  $f(x) > 0$  over  $[0, 1]$ . If  $f(x) < 0$  at some region, we can add a constant shift  $C$  as large as needed to render  $f(x)$  positive. For the  $i^{\text{th}}$  neuron  $R_i$ , its output is expressed as:

$$R_i = (W_i x + b_i)^+, \quad (4)$$

where  $+$  denotes a ReLU operation,  $W_i$  and  $b_i$  are weight and bias respectively. In the following, mathematical induction is used to show that our construction can express  $f(x)$  exactly.

**Initial Condition  $R_0$ :** We use  $R_0$  to implement the linear function in the first interval  $[x_0, x_1]$ . By setting  $W_0 = \left| \frac{f(x_1)-f(x_0)}{x_1-x_0} \right|$ ,  $b_0 = \left| \frac{f(x_1)-f(x_0)}{x_1-x_0} \right| x_0$ , the specific function of the first neuron becomes:

$$R_0 = \left( \left| \frac{f(x_1)-f(x_0)}{x_1-x_0} \right| (x-x_0) \right)^+, \quad (5)$$

where the ReLU keeps the linearity when  $x > x_0$ .

**Recurrent Relation:** Suppose that we have obtained the desired  $i^{\text{th}}$  neuron  $R_i$ , we can proceed to design the  $(i+1)^{\text{th}}$  neuron with the goal to express the function  $|f_{i+1}(x) - f_{i+1}(x_{i+1})|$  over the interval  $[x_{i+1}, x_{i+2}]$ , which is  $|f(x)|$  without a constant lift. The tricky point is that the current neuron basically takes in the output of the previous neuron as the input, which is in the functional range instead of the input domain. Therefore, we need to perform an inverse affine transform.

For convenience, we define  $M_{i+1} = \frac{f(x_{i+2})-f(x_{i+1})}{x_{i+2}-x_{i+1}}$  and

$M_i = \frac{f(x_{i+1}) - f(x_i)}{x_{i+1} - x_i}$ , where  $i \geq 0$ .

$$R_{i+1} = \left( |M_{i+1} - M_i| \times \left( \frac{1}{|M_i - M_{i-1}|} R_i - x_{i+1} + x_i \right) \right)^+ \quad (6)$$

For notation completeness,  $M_{-1} = 0$ . The trick we use is to invert  $R_i$  back to the input domain and set the new slope as  $|M_{i+1} - M_i|$ , which cancels the effect of  $R_i$  imposed on  $x > x_{i+1}$ , equivalently limiting  $R_i$  to only work over  $[x_i, x_{i+1}]$  once  $R_i$  and  $R_{i+1}$  are added together. The parameters in the  $(i+1)^{th}$  module are chosen as follows:  $W_{i+1} = \frac{|M_{i+1} - M_i|}{|M_i - M_{i-1}|}$  and  $b_{i+1} = (-x_{i+1} + x_i)|M_{i+1} - M_i|$ .

Thanks to the recurrent relation, each  $R_i$  can accurately represent a small monotonically increasing piece over  $[x_i, x_{i+1}]$ . We aggregate the outputs of those  $L$  pieces in the final neuron as

$$\sum_{i=0}^{L-1} \text{sgn}(i) R_i + f(x_0), \quad (7)$$

wherein  $\text{sgn}(i) = 1$  when  $M_i - M_{i-1} > 0$  and  $\text{sgn}(i) = -1$  when  $M_i - M_{i-1} < 0$ . Eq. (7) can perfectly denote the  $f(x)$ . To illustrate the idea clearly, we exemplify  $\sum_{i=0}^2 \text{sgn}(i) R_i + f(x_0)$  as  $R_0 + R_1 - R_2 + f(x_0)$ , as shown in Figure 2.

Based on the above derivation, for any  $f(x)$  consisting of  $L$  piecewise linear segments and the first piece is non-constant, there will be a function  $\sum_{i=0}^{L-1} R_i$  constructed by a one-neuron-wide L-layer S3-Net that can exactly represent  $f(x)$ . Because  $f(x)$  can approximate any continuous univariate function, it is concluded that any continuous univariate function can be expressed by a one-neuron-wide deep S3-Net. This immediately verifies our proposition.

**Remark 1:** Although one neuron per layer is sufficient for the S3-Net to have a good expressive ability, a typical network usually uses shortcuts to interconnect the outputs of network blocks, which will offer even more expressive abilities. The necessity of dense connections in the DenseNet is generally counter-intuitive, as it involves too many parameters during internal aggregation. A natural question is whether such dense connections are really needed or not. [35] experimentally demonstrated in some extent that a densely connected structure is not an optimal design, while our proposition theoretically makes sure that considerable redundancy truly exists in DenseNet. To the best of our knowledge, theoretical results illustrating the representation power of shortcut connections is scarce, if not totally absent. Our result with S3-Net topology, together with [32], justify the power of shortcuts in terms of capacity. That is, with the shortcut connections, the network can be extremely slim (one neuron per layer) for general approximation.

**Example:** Figure 3 shows a simple example wherein a one-neuron S3 network with 10 layers is trained to fit the univariate function  $h(x) = x^3 - 0.25x + 0.2$ . The data are synthesized by sampling from  $[1, 2]$  with the interval of 0.01. The highlight is that S3-Net well fits the  $h(x)$  over the support.

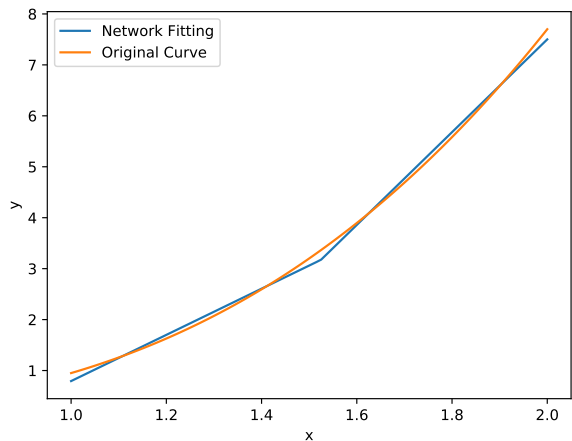


Fig. 3. One-neuron S3-Net with 10 layers can approximate  $h(x) = x^3 - 0.25x + 0.2$  over  $[1, 2]$  well.

### III. WIDTH-BOUNDED UNIVERSAL APPROXIMATOR

Inspired by the feasibility of using a one-neuron-wide S3-Net to approximate any continuous univariate function, here we present an alternative width-bounded universal approximator, in analogue to a depth-bounded universal approximator. Width-bounded networks mean the width of network is limited but the network can be arbitrarily deep. Our scheme is based on the S3-Net topology and the Kolmogorov-Arnold representation theorem. Specifically, we employ the Kolmogorov-Arnold representation theorem to bridge the gap between approximating univariate and multivariate functions.

**Conjecture 2:** With the ReLU activation, for any continuous function  $f : [0, 1]^n \rightarrow \mathbb{R}$  and any given precision  $\sigma > 0$ , there exists a neural network  $W$  with width no more than  $2n^2 + n$  such that

$$\sup_{x_1, x_2, \dots, x_n \in [0, 1]} |f(x_1, x_2, \dots, x_n) - W(x_1, x_2, \dots, x_n)| < \sigma, \quad (8)$$

**Kolmogorov-Arnold representation theorem** [29]: According to the Kolmogorov-Arnold representation theorem, for any continuous function  $f(x_1, \dots, x_n)$  with  $n \geq 2$ , there exists a group of continuous functions:  $\phi_{q,p}, q = 0, 1, \dots, 2n; p = 1, 2, \dots, n$  and  $\Phi_q$  such that

$$f(x_1, x_2, \dots, x_n) = \sum_{q=0}^{2n} \Phi_q \left( \sum_{p=1}^n \phi_{q,p}(x_p) \right). \quad (9)$$

**Scheme of analysis:** The representation theorem implies that any continuous function  $f(x_1, \dots, x_n)$  can be written as a composition of finitely many univariate functions. As shown in Figure 3, our scheme of approximating a multivariate continuous function  $f(x_1, \dots, x_n)$  is to first employ  $2n^2 + n$  single-neuron-wide S3-Net to represent  $\phi_{q,p}(x_p)$  in a parallel manner. Next, suggested by the right side of Eq. (9), we summate the group of functions  $\{\phi_{q,1}(x_1), \phi_{q,2}(x_2), \dots, \phi_{q,n}(x_n)\}$  and feed  $\sum_{p=1}^n \phi_{q,p}(x_p)$  into a new one-neuron-wide S3-Net whose purpose is to approximate  $\Phi_q$ . Finally, we summate the yields of those

$2n + 1$  sub-networks as the ultimate output of the overall network.

**Analysis:** As we have shown in the preceding section, for every function  $\phi_{q,p}(x_p)$ , there exists a function  $D_{q,p}(x_p)$  represented by a one-neuron-wide S3-Net such that:

$$\sup_{x_p \in [0,1]} |\phi_{q,p}(x_p) - D_{q,p}(x_p)| < \delta_{q,p}, \quad (10)$$

where  $\delta_{q,p}$  is given arbitrarily small quantity. After we integrate  $\{\phi_{q,1}(x_1), \phi_{q,2}(x_2), \dots, \phi_{q,n}(x_n)\}$ , for any selection of  $x_1, x_2, \dots, x_n \in [0, 1]$ , we have:

$$\begin{aligned} & \sup_{x_1, x_2, \dots, x_n \in [0,1]} \left| \sum_{p=1}^n \phi_{q,p}(x_p) - \sum_{p=1}^n D_{q,p}(x_p) \right| \\ & < \sup_{x_1, x_2, \dots, x_n \in [0,1]} \sum_{p=1}^n |\phi_{q,p}(x_p) - D_{q,p}(x_p)| \quad (11) \\ & < \sum_{p=1}^n \delta_{q,p}. \end{aligned}$$

Given that  $\Phi_q$  is continuous, we employ the  $\epsilon - \delta$  definition of continuity: if  $g(x)$  is continuous at  $x_0$ , then for any positive number  $\epsilon$ , there exists  $\delta(\epsilon, g) > 0$  satisfying that  $|g(x) - g(x_0)| < \epsilon$  when  $|x - x_0| < \delta$ . Let  $\epsilon = \frac{\sigma}{4n+2}$ , correspondingly we appropriately choose  $\delta_{q,p}$  so that  $\sum_{p=1}^n \delta_{q,p} < \delta(\frac{\sigma}{4n+2}, \Phi_q)$ . In this case, for every  $\Phi_q$ , we have the following:

$$\begin{aligned} & \sup_{x_1, x_2, \dots, x_n \in [0,1]} \left| \Phi_q\left(\sum_{p=1}^n \phi_{q,p}(x_p)\right) - \Phi_q\left(\sum_{p=1}^n D_{q,p}(x_p)\right) \right| \\ & < \frac{\sigma}{4n+2}. \quad (12) \end{aligned}$$

For every continuous function  $\Phi_q$ , it is supported on  $\mathbb{R}$  instead of  $[0, 1]$ . Without loss of generality, we can still find an one-neuron-wide S3-Net to approximate  $\Phi_q$ . Let  $D_q(x)$  be the function expressed by a one-neuron-wide S3-Net, we have:

$$\sup_{x \in \mathbb{R}} |\Phi_q(x) - D_q(x)| < \frac{\sigma}{4n+2}. \quad (13)$$

Eq. (13) means that  $D_q(x)$  can represent  $\Phi_q(x)$  with an error no greater than  $\frac{\sigma}{4n+2}$  over  $\mathbb{R}$ . Applying the triangle inequality, we have

$$\begin{aligned} & \sup_{x_1, x_2, \dots, x_n \in [0,1]} \left| \Phi_q\left(\sum_{p=1}^n \phi_{q,p}(x_p)\right) - D_q\left(\sum_{p=1}^n D_{q,p}(x_p)\right) \right| \\ & < \sup_{x_1, x_2, \dots, x_n \in [0,1]} \left| \Phi_q\left(\sum_{p=1}^n \phi_{q,p}(x_p)\right) - \Phi_q\left(\sum_{p=1}^n D_{q,p}(x_p)\right) \right| \\ & + \sup_{x_1, x_2, \dots, x_n \in [0,1]} \left| \Phi_q\left(\sum_{p=1}^n D_{q,p}(x_p)\right) - D_q\left(\sum_{p=1}^n D_{q,p}(x_p)\right) \right| \\ & < \frac{\sigma}{2n+1}. \quad (14) \end{aligned}$$

From Eq. (14), by applying the triangle inequality again, we immediately obtain that:

$$\begin{aligned} & \sup_{x_1, x_2, \dots, x_n \in [0,1]} \left| \sum_{q=0}^{2n} \Phi_q\left(\sum_{p=1}^n \phi_{q,p}(x_p)\right) - \sum_{q=0}^{2n} D_q\left(\sum_{p=1}^n D_{q,p}(x_p)\right) \right| \\ & \leq \sup_{x_1, x_2, \dots, x_n \in [0,1]} \sum_{q=0}^{2n} \left| \Phi_q\left(\sum_{p=1}^n \phi_{q,p}(x_p)\right) - D_q\left(\sum_{p=1}^n D_{q,p}(x_p)\right) \right| \\ & < \sigma. \quad (15) \end{aligned}$$

Let  $W(x_1, x_2, \dots, x_n) = \sum_{q=0}^{2n} D_q(\sum_{p=1}^n D_{q,p}(x_p))$ , we immediately arrive at our conjecture. Thus, the  $(2n^2 + n)$ -width bounded network can represent the  $f(x_1, x_2, \dots, x_n)$  with any precision.

**Remark 2:** Here, we present a novel width-limited universal approximator with the width no more than  $2n^2 + n$ . In contrast to other width-bounded universal approximators, the construction here jointly manifests the power of deep networks and the power of shortcuts. In particular, due to the scarcity of width-bounded universal approximators [30], our work still makes sense despite that the width bound in our construction is greater than  $n + 4$  in [30] and 1 in [32].

#### IV. EQUIVALENT NETWORKS AND THEIR SPECTRAL CHARACTERIZATION

Motivated by our constructive proof for one-neuron S3-Net topology, we report that in one-dimension setting, the aforementioned analysis is translatable to a rather inclusive family of networks. These networks are characterized by a kind of topology ( $\Omega^N$ ) that subsumes an extremely wide network, an extremely deep network and networks between them, where  $N$  is the number of neurons including the input node. By showing the approximation capability of this family of networks, we argue that those networks are equivalent. We further justify the network equivalency through statistical significance experiments. Finally, we present the spectral characterization for  $\Omega^N$ .

The input node is also considered as the neuron for simplicity. Hence define the hidden neurons, input neuron and output neuron. The network family  $\Omega^N$  satisfies the following three requirements:

- (1) Every hidden neuron has one inbound edge.
- (2) Every hidden neuron and the input neuron have one outbound edge that links to the output neuron.
- (3) The input is wired with at least one hidden neuron.

Later, we will illustrate that (1) can be relaxed to that every hidden neuron has at least one inbound edge. The examples that belong to  $\Omega^8$  are shown in Figure 5. To fulfill such topology, the number of required edges should be  $2N - 3$  if  $N$  is the number of neurons. One thing worthwhile to highlight is that the members in  $\Omega^N$  are mutually convertible through one or more cutting-rewiring operations. A cutting-rewiring operation means that cutting the current input edge of one neuron and rewiring the one with some other neuron, which will not impact the expressive power. Regarding the network belonging to family  $\Omega$ , we have the following conjecture: In terms of the  $L^\infty$  distance, there exists an  $N$  such that any

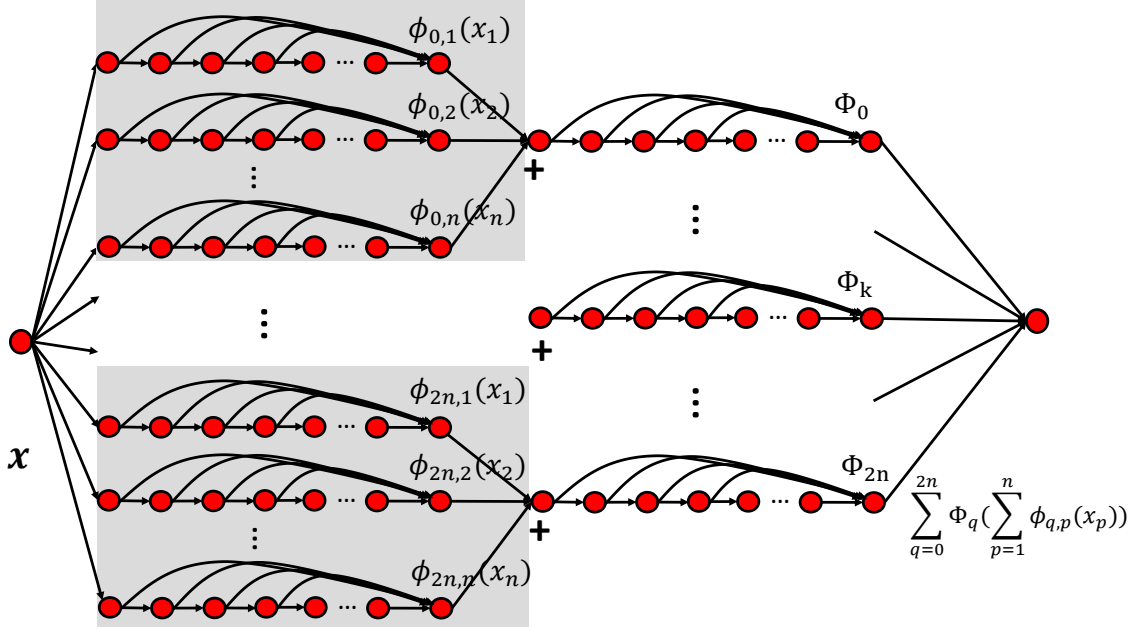


Fig. 4. The scheme of a width-bounded universal approximator.

network in  $\Omega^{N+2}$  using ReLU as activation functions can approximate any continuous univariate function.

**Conjecture 3:** With ReLU activation, for any continuous function  $g : [0, 1] \rightarrow \mathbb{R}$  and any given precision  $\delta > 0$ , there is an  $N$  such that any network  $K$  of  $\Omega^{N+2}$  whose mapping is denoted as  $\Omega_K^{N+2}(x)$  satisfies:

$$\sup_{x \in [0,1]} |g(x) - \Omega_K^{N+2}(x)| < \delta. \quad (16)$$

**The sketch of analysis:** Similarly, for a univariate continuous function, it will be well approximated by a continuous  $N$  piecewise linear function. Therefore, the problem becomes how to represent a continuous piecewise function by a network from the  $\Omega^{N+2}(x)$ . Again, our strategy is to drive each neuron to represent a concerning segment and then we use shortcut connections to aggregate these linear segments in the output neuron. This is the reason why we need the second requirement. The core technique is that the hidden neuron is allowed to get the information from any previous neurons other than just from the exact previous neighboring neuron.

**Analysis:** Here, for convenience and without loss of generality, we still use  $f(x)$  in Eq. (2) but let  $L = N$ . To arrive Conjecture 3, we need to use  $\Omega_K^{N+2}(x)$  to express  $f(x)$  for construction.

Now we show how weights and bias in each neuron are appropriately selected in  $\Omega_K^{N+2}(x)$  to approximate  $f(x)$ . Without loss of generality, the neurons are denoted as  $Q_{input}, Q_0, \dots, Q_{N-1}, Q_{output}$ , where  $Q_{input}$  is the input node,  $Q_0$  is connected to the input neuron directly and  $Q_{i+1}$  is fed with either the input neuron or some neuron  $Q_t, t \leq i$ , and  $Q_{output}$  is the output neuron. Accordingly, the outputs of neurons  $Q_0, Q_1, \dots, Q_{N-1}$  are also

denoted as  $Q_0, Q_1, \dots, Q_{N-1}$  for convenience, and our goal is to let  $Q_0, Q_1, \dots, Q_{N-1}$  to represent  $f_0, f_1, f_2, \dots, f_{N-1}$  at  $[x_0, x_1], [x_1, x_2], \dots, [x_{N-1}, x_N]$  respectively. We also assume  $f(x) > 0$  over  $[0, 1]$ , which is plausible because if  $f(x) < 0$  for some  $x$ , we can add a sufficiently large shift  $C$  at beginning, and then compensate  $-C$  at the output neuron. The inner-making calculation in each neuron is formulated as:

$$Q_i = (W_i x + b_i)^+, \quad (17)$$

where  $+$  means a *ReLU* operation for short.  $W$  and  $b$  are weight and bias in the neuron.

$Q_0$ : We utilize  $Q_0$  to implement the piece in the first interval  $[x_0, x_1], x_0 = 0$ . By setting  $W_0 = \left| \frac{f(x_1) - f(x_0)}{x_1 - x_0} \right|, b_0 = \left| \frac{f(x_1) - f(x_0)}{x_1 - x_0} \right| x_0$ , the specific function of the first neuron becomes:

$$Q_0 = \left( \left| \frac{f(x_1) - f(x_0)}{x_1 - x_0} \right| (x - x_0) \right)^+, \quad (18)$$

where ReLU keeps the linearity for  $x > x_0$ .

$Q_{i+1}$ : As far as  $Q_{i+1}$  is concerned, there are two situations: the neuron  $Q_{i+1}$  is wired with the neuron  $Q_j$  or with the input neuron.

For the first situation, suppose that  $j^{th}$  neuron  $Q_j$  desirably denotes the segment at the interval  $[x_j, x_{j+1}]$ , we proceed to devise the  $(i+1)^{th}$  neuron to express the segment over the interval  $[x_{i+1}, x_{i+2}]$  without a constant lift. Again, the bullet point is that we need to perform an inverse affine transform because the output of the previous neuron is in the functional domain instead of the input domain. Let  $M_{-1} = 0$

TABLE I  
ERROR RATE OF THE SIX NETWORKS IN 20 RANDOM INITIALIZATIONS.

	Network I	Network II	Network III	Network IV	Network V	Network VI
1	0.1084	0.1078	0.0990	0.1075	0.0996	0.1039
2	0.1039	0.1052	0.0990	0.1017	0.1005	0.1046
3	0.1015	0.1062	0.1041	0.1050	0.1046	0.1032
4	0.0993	0.1034	0.1063	0.1054	0.1013	0.1034
5	0.1042	0.1081	0.1073	0.1092	0.1023	0.1065
6	0.1076	0.1020	0.1007	0.1073	0.1092	0.1038
7	0.1073	0.1042	0.0975	0.1065	0.1067	0.1015
8	0.1037	0.1082	0.1088	0.1051	0.1068	0.1035
9	0.1088	0.1031	0.1021	0.1054	0.1072	0.1079
10	0.1033	0.1043	0.1059	0.1059	0.1014	0.1013
11	0.1086	0.1047	0.0999	0.1030	0.1041	0.1073
12	0.1094	0.1065	0.1024	0.0994	0.1085	0.1040
13	0.1070	0.1031	0.1027	0.1106	0.1050	0.1013
14	0.1002	0.1034	0.1084	0.1030	0.1013	0.1067
15	0.1071	0.1061	0.1018	0.1050	0.1033	0.1042
16	0.0993	0.1031	0.1031	0.1019	0.1020	0.1046
17	0.1044	0.1037	0.1054	0.0990	0.1056	0.1078
18	0.1073	0.1068	0.1023	0.1071	0.1031	0.1031
19	0.1084	0.1016	0.1063	0.1015	0.1041	0.1016
20	0.1009	0.1063	0.1026	0.1111	0.1050	0.1013
mean	0.1050	0.1049	0.1033	0.1050	0.1039	0.1044

for completeness and because  $M_{i+1} \neq M_i, i \geq 0$ , we have:

$$Q_{i+1} = \left( |M_{i+1} - M_i| \times \left( \frac{1}{|M_j - M_{j-1}|} Q_j - x_{i+1} + x_j \right) \right)^+, \quad (19)$$

The inverse affine transform can invert  $Q_j$  back to the input domain and set the new slope as  $|M_{i+1} - M_i|$ . This counteracts the effect of  $Q_i$  at  $x > x_{i+1}$ , equivalently squeezing  $Q_i$  only for  $[x_i, x_{i+1}]$  when  $Q_i$  and  $Q_{i+1}$  are added together. The parameters in the  $Q_{i+1}$  are chosen as follows:  $W_{i+1} = \frac{|M_{i+1} - M_i|}{|M_j - M_{j-1}|}$  and  $b_{i+1} = (-x_{i+1} + x_j)|M_{i+1} - M_i|$ .

For the second case, no inverse affine transform is required,

$$Q_{i+1} = (|M_{i+1} - M_i| \times (x - x_{i+1}))^+, \quad (20)$$

where the weights and bias are respectively selected as:  $W_{i+1} = |M_{i+1} - M_i|$  and  $b_{i+1} = -|M_{i+1} - M_i|x_{i+1}$ .

Thanks to the above recurrent relation, each  $Q_{i+1} + Q_i$  manages to accurately represent absolute value of a small non-negative piece over  $[x_{i+1}, x_i]$ . We aggregate the output of all  $N$  pieces in the final neuron as

$$\sum_{i=0}^{N-1} \text{sgn}(i)Q_i + f(x_0), \quad (21)$$

wherein  $\text{sgn}(i) = 1$  when  $M_{i+1} - M_i > 0$  and  $\text{sgn}(i) = -1$  when  $M_{i+1} - M_i < 0$ . The Eq. 21 can perfectly express the  $f(x)$ .

**Remark 3:** In the framework of the network family  $\Omega$ , our representation ability analysis suggests that the members of  $\Omega$  are actually equivalent. We would like to emphasize such finding is important in both theoretical and practical senses. 1) Previously, both a one-hidden-layer but super wide network and a one-neuron-wide but super deep network were demonstrated to have strong expressive ability. A natural curiosity is what about the networks in between. Are they

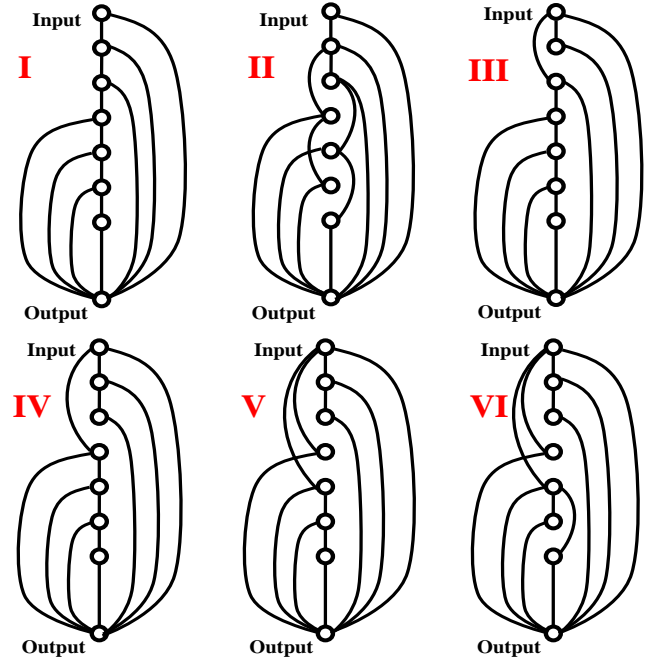


Fig. 5. Six exemplary structures in  $\Omega^8$  combined with ResNet setup were used to test if the networks in  $\Omega$  are truly equivalent or not.

also permitting a good approximation ability? Here, we partially answer this question in one dimension setting since the network family  $\Omega$  comprises of a wide network, a deep network and networks in between. They are equally capable in terms of approximating a univariate function. 2) Network design is an important research direction. Changing where to take inputs makes no impact on the approximation ability of the network, by which the insight can be drawn to network architecture design and search. Since we discovered that a good amount of networks are actually equivalent to each other, the search and design cost will be much

TABLE II  
THE P-VALUES BETWEEN EXPERIMENTAL RESULTS OF ALL THE PAIRED NETWORKS.

	Network I	Network II	Network III	Network IV	Network V	Network VI
Network I		0.8765	0.1030	1	0.2723	0.4743
Network II			0.0671	0.8738	0.2179	0.4439
Network III				0.1007	0.4857	0.2179
Network IV					0.2684	0.4701
Network V						0.5856

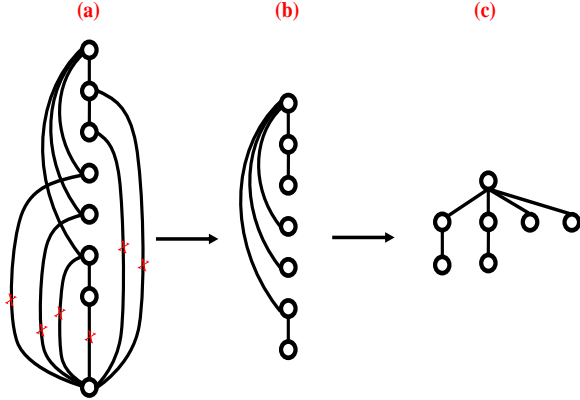


Fig. 6. The network in family  $\Omega$  is a tree by deleting output neuron-related connections,

reduced in principle considering the shortcut topology is essential in neural architecture search and design. Also, the network family  $\Omega$  somehow indicates a family of simplest networks since the connections between non-output neurons are indispensable, meaning if cutting one connection, one or several neurons got isolated. In this regard, our constructive analysis provides an approach in discriminating redundant networks.

**Experiment:** Here, we evaluate the classification performances on CIFAR-10 to examine whether the networks in  $\Omega$  are truly equivalent or not. Here, the shortcuts are used as summation. We constructed the network by combining the setup of ResNet [40] and the shortcut design by  $\Omega$ . The ResNet comprises of three stages with feature maps of sizes 32, 16 and 8. All the network machineries were kept intact instead of the shortcut topology of three stages, which were replaced as the topology in  $\Omega$ . We randomly picked up six structures from  $\Omega^8$  for the structure of each stage as shown in Figure 6. The training procedure also followed the setup in [40]. Table I shows the performance of Network I-VI on benchmark CIFAR-10 in 20 random initialization. It can be seen that the mean error rates of six networks are quite close to each other, the maximum difference is 0.17%, which indicates that the six networks perform similarly. To rigorously justify, we implemented the independent samples t-test, and the null hypothesis is that data in two groups are from populations with equal means, without assuming that the populations also have equal variances. The obtained p-values between results of any two networks are shown in Table II. The lowest p-value 6.17% is from the results

of networks III and IV, which is not sufficiently low (the bar is 5%) to reject that the networks III and IV behave differently. Thus, the network equivalency suggested from representational analysis is demonstrated.

**Spectral Characterization:** Let  $G = (V, E)$  be an undirected graph with  $N$  vertices denoted as  $v_1, v_2, \dots, v_N$ . Let  $A$  be the adjacency matrix of  $G$  and  $A_{ij} = 1$  if  $v_i$  and  $v_j$  is connected. Otherwise,  $A_{ij} = 0$ . The largest eigenvalue  $\rho$  of  $A$  is often called the spectral radius of  $G$ . A neural network is a directed graph but here we ignore the direction of the edge for simplicity. There is a special kind of graph called a tree which is defined as:  $G$  is a tree  $T$  if  $G$  is connected and has  $n - 1$  edges. We find that by deleting output neuron-related connections, the network in family  $\Omega$  fulfills the definition of a tree (as Figure 6 shown). We use  $G(\Omega)$  to denote the graphs that corresponds to the network in  $\Omega$  discarding the output neuron and associated edges. Such deletion is reasonable since all the members in  $\Omega$  shares this part. Further, if a node is directly connected to other nodes in a tree, then such a tree is called a star. Regarding the tree and the star, we have the following theorem.

Collatz and Sinogowitz [49]: If  $G$  is a tree with  $n$  vertices, then  $\rho \leq n - 1$ . The upper bounds occurs only when  $G$  is a star.

In other words, the maximum spectral radius is achieved when a tree is a star, which corresponds to a one-hidden-layer wide network. Therefore, the spectral radius of the  $G(\Omega^{N+2})$  is no more than  $N$ .

## V. GENERALIZATION BOUND ANALYSIS

For the basic topology of S3-Net, there are two types of aggregations for shortcuts: addition (+) like residual networks and the concatenation ( $\oplus$ ) like the DenseNet. In this section, we first demonstrate the margin-based multi-class generalization bound of DenseNet, then we compare the margin-based multi-class generalization bounds of the S3-Net and DenseNet. Next, on top of the margin-based multi-class generalization bound, we also investigate the generalization bounds of other forms for the DenseNet, and by the same trick it can be shown that the generalization bounds of the S3-Net are tighter than those of the DenseNet. Finally, as an evaluation to generalization bounds, we demonstrated the superiority of DenseNet with classification experiments on CIFAR-100. To the best of our knowledge, quite few theoretical analysis was performed on the effect of concatenation connections on the generalization ability of deep networks, which makes our analysis novel.



Let us assume that data norm is set to the  $l_2$  norm and the operator norm set to the spectral norm  $\|\cdot\|_\sigma$ , where  $\|\cdot\|_\sigma$  is defined as  $\|A\|_\sigma = \sup_{\|Z\|_2 \leq 1} \|AZ\|_2$ . Furthermore,  $\|\cdot\|_{p,q}$  is the matrix norm defined as  $\|A\|_{p,q} = \|(\|A_{:,1}\|_p, \dots, \|A_{:,m_2}\|_p)\|_q$  for  $A \in \mathbb{R}^{m_1 \times m_2}$ .

Next, we define the margin operator  $\mathcal{M}$  for the  $k$ -class classification task as  $\mathcal{M} : \mathbb{R}^k \times \{1, 2, \dots, k\} \rightarrow \mathbb{R}$  and the ramp function is:

$$l_\gamma(r) = \begin{cases} 0 & r < -\gamma \\ 1 + r/\gamma & -\gamma \leq r \leq 0 \\ 1 & r > 0, \end{cases} \quad (22)$$

where  $\gamma$  is the margin controlling the slope of  $l_\gamma(r)$ . Then, the empirical ramp loss over the dataset  $D = \{(x_1, y_1), \dots, (x_n, y_n)\}$  is

$$\hat{\mathcal{R}}_\gamma(F) = \frac{1}{n} \sum_{i=1}^n (l_\gamma(-\mathcal{M}(F(x_i), y_i))), \quad (23)$$

while the expected test error with respect to the hypothesis space  $F$  under the 0-1 loss is

$$Pr\{\arg \max_i F(x_i) \neq y\}, \quad (24)$$

where  $x$  is an input and  $y$  is the corresponding label.

With all the notations and definitions, we have the following Theorem 1.

**Theorem 1:** Let us fix nonlinear activation functions  $\sigma_1, \dots, \sigma_L$  where  $\sigma_i$  is  $\rho_i$ -Lipschitz and  $\sigma_i(0) = 0$ . Further, let margin  $\gamma > 0$ , data bound  $B$ , spectral norm bounds  $(s_1, \dots, s_L)$  and matrices (2, 1) norm bounds  $(b_1, \dots, b_L)$  be given. Then, with at least  $1 - \delta$  probability over  $N$  samples  $((x_i, y_i)_{i=1}^N)$  with  $x_i \in \mathbb{R}^d$ ,  $\sqrt{\sum_i \|x_i\|_2^2} \leq B$  are drawn from identical and independent distribution, every DenseNet in  $F_A : \mathbb{R}^d \rightarrow \mathbb{R}^k$  defined as

$$\begin{cases} G_0 = X^T \\ F_1 = A_1 X^T \\ G_i = \sigma_i(F_i) \\ F_{i+1} = A_{i+1} \oplus_{k=0}^i G_k \\ F_L = A_L \oplus_{k=0}^{L-1} G_k \end{cases} \quad (25)$$

where  $\oplus$  is the matrix concatenation along the column direction,  $\oplus_{k=0}^i G_k = G_1 \oplus G_2 \cdots \oplus G_k = [G_0; G_1; \dots; G_k]$ ,  $A_i$  is of  $d_i \times n_i$ ,  $n_i = \sum_{k=0}^{i-1} d_k$  and  $X \in \mathbb{R}^{N \times d}$  collects data samples, the matrices  $\mathcal{A} = (A_1, \dots, A_L)$ ,  $A_i \in \mathbb{R}^{d_i \times n_i}$ ,  $n_i = \sum_{k=0}^{i-1} d_k$  obey that  $\|A_i\|_\sigma \leq s_i$  and  $\|A_i^T\|_{2,1} \leq b_i$  satisfies:

$$\begin{aligned} & Pr\{\arg \max_i F_A(x_i) \neq y\} - \hat{\mathcal{R}}_\gamma(F_A) \\ & \leq \frac{8}{n^{3/2}} + 3\sqrt{\frac{\ln(1/\delta)}{2n}} + \\ & \frac{36B \ln(n) \prod_{j=1}^L (1 + \rho_j s_j)}{\gamma n} \sqrt{\sum_{i=1}^L \frac{\rho_i^2 b_i^2}{(1 + \rho_j s_j)^2} \sum_{i=1}^L \ln(2d_i n_i)}. \end{aligned} \quad (26)$$

**Remark 4:** The above result is the margin-based multi-class generalization bound regarding  $L$ -layer DenseNet. For

conciseness, we put its proof in the Appendix. Please note that our results are based on the proof about chain-like networks in [36], and our main contribution is to apply the results on the chain-like networks into the networks with concatenation shortcuts, thereby casting light on the impact of concatenation shortcuts on the generalization bound of deep networks. Due to the wide applications of networks with concatenation shortcuts, our work is still valuable. In our formulation, concatenating the outputs from previous layers are realized as the matrix concatenation in Eq. (19). From Eq. (19), it can be deduced that the incorporation of dense concatenation shortcuts indeed lead to a worse generalization ability due to the increased matrix size  $n_i = \sum_{k=0}^{i-1} d_k$ , which agrees with Occam's razor. In contrast, He *et al.* [34] analyzed the generalization ability of the ResNet based on [36] as well, it turns out that the ResNet has proximal generalization bound with the chain-like networks.

Next, we also derive the margin-based multi-class generalization bound of S3-Net( $\oplus$ ) and compare it with that of the DenseNet. To discriminate the results of S3-Net( $\oplus$ ), in the following we use the superscript ( $D$ ) to denote the parameters pertaining to DenseNet and the superscript ( $S$ ) for the parameters pertaining to S3-Net( $\oplus$ ). Therefore, Eq. (20) turns into

$$\begin{aligned} & Pr\{\arg \max_i F_A^{(D)}(x_i) \neq y\} - \hat{\mathcal{R}}_\gamma(F_A^{(D)}) \\ & \leq \frac{8}{n^{3/2}} + 3\sqrt{\frac{\ln(1/\delta)}{2n}} + \\ & \frac{36B \ln(n) \prod_{i=1}^L (1 + \rho_i s_i^{(D)})}{\gamma n} \sqrt{\sum_{i=1}^L \frac{\rho_i^2 b_i^{(D)2}}{(1 + \rho_i s_i^{(D)})^2} \sum_{i=1}^L \ln(2d_i n_i^{(D)})}. \end{aligned} \quad (27)$$

For a fair comparison, we set the output dimension of each layer in S3Net( $\oplus$ ) to the same as that of the DenseNet. Also, we use  $d_i$  for both networks. Let  $A_i^{(S)}$  be of  $d_i \times n_i^{(S)}$ , where  $n_i^{(S)} = d_{i-1}$ ,  $i \leq L-1$ ,  $n_L^{(S)} = \sum_{i=1}^{L-1} d_i$  and  $X \in \mathbb{R}^{N \times d}$ . The computational structure of S3-Net( $\oplus$ ) is

$$\begin{cases} G_0^{(S)} = X^T \\ F_1^{(S)} = A_1^{(S)} X^T \in \mathcal{W}_2 \\ G_i^{(S)} = \sigma_i(F_i^{(S)}) \\ F_{i+1}^{(S)} = A_{i+1}^{(S)} G_i^{(S)}, i \leq L-2 \\ F_L^{(S)} = A_L^{(S)} \oplus_{k=0}^{L-1} G_k^{(S)}. \end{cases} \quad (28)$$

Without changing the final output, we can rewrite the computational structure of S3-Net equivalently with zero padding as:

$$\begin{cases} G_0^{(S)} = X^T \\ F_1^{(S)} = A_1^{(S)} Z \in \mathcal{W}_2 \\ G_i^{(S)} = \sigma_i(F_i^{(S)}) \\ F_{i+1}^{(S)} = [A_{i+1}^{(S)}, \mathbf{0}^{d_{i+1} \times \sum_{k=0}^i d_k}] [G_i^{(S)}; \mathbf{0}^{d_i \times n_i}; \dots; \mathbf{0}^{d_0 \times n_i}] \\ F_L^{(S)} = A_L^{(S)} \oplus_{k=0}^{L-1} G_k^{(S)}, \end{cases} \quad (29)$$

where  $\mathbf{0}^{C_1 \times C_2}$  means the zero matrix of  $C_1 \times C_2$ . Because zero padding operations only influence the size of a matrix without impacting spectral norm bounds ( $s_1^{(S)}, \dots, s_L^{(S)}$ ) and  $l_1$  norm bounds ( $b_1^{(S)}, \dots, b_L^{(S)}$ ), we can construct the generalization bound for the above zero-padded S3-Net by mimicking the DenseNet:

$$\begin{aligned} & Pr\{\arg \max_i F_{\mathcal{A}}^{(S)}(x)_i \neq y\} - \hat{\mathcal{R}}_\gamma(F_{\mathcal{A}}^{(S)}) \\ & \leq \frac{8}{n^{3/2}} + 3\sqrt{\frac{\ln(1/\delta)}{2n}} + \\ & \frac{36B\ln(n) \prod_{i=1}^L (1 + \rho_i s_i^{(S)})}{\gamma n} \sqrt{\sum_{i=1}^L \frac{\rho_i^2 b_i^{(S)2}}{(1 + \rho_i s_i^{(S)})^2} \sum_{i=1}^L \ln(2d_i n_i^{(D)})}, \end{aligned} \quad (30)$$

where we notice  $n_i^{(D)}$  is used because the matrix has been enlarged.

**Conjecture 4:** The margin-based multi-class generalization bound of the S3-Net( $\oplus$ ) is tighter than that of the DenseNet.

**Analysis:** Apparently, the fact holds that:

$$n_i^{(S)} \leq n_i^{(D)}, i = 1, 2, \dots, L. \quad (31)$$

In other words, the matrix  $A_i^{(D)}$  is always not smaller than  $A_i^{(S)}$  along any axis. As a consequence, according to the definition of spectral norm, we have:

$$\begin{aligned} & \|A_i^{(S)}\|_\sigma \\ & = \sup_{\|Z\|_2 \leq 1} \|A_i^{(S)} Z^{(S)}\|_2 \\ & = \sup_{\|Z\|_2 \leq 1} \|[A_i^{(S)}, \mathbf{0}^{d_i \times (n_i^{(D)} - n_i^{(S)})}]\| \|[Z; \mathbf{0}^{(n_i^{(D)} - n_i^{(S)}) \times n}]\|_2 \\ & \leq \sup_{\|Z\|_2 \leq 1} \|A_i^{(D)} Z^{(D)}\|_2 \\ & = \|A_i^{(D)}\|_\sigma, \end{aligned} \quad (32)$$

where zero padding is of  $\mathbb{R}^{d_i \times (n_i^{(D)} - n_i^{(S)})}$  to render  $[A_i^{(S)}, \mathbf{0}]$  have the same size as that of  $A_i^{(D)}$ . Therefore we derive that

$$s_i^{(S)} \leq s_i^{(D)}, i = 1, \dots, L. \quad (33)$$

In the same spirit, we can also derive that:

$$b_i^{(S)} \leq b_i^{(D)}, i = 1, \dots, L. \quad (34)$$

Combining Eqs. (32)-(34), we have:

$$\begin{aligned} & \prod_{i=1}^L (1 + \rho_i s_i^{(S)}) \sqrt{\sum_{i=1}^L \frac{\rho_i^2 b_i^{(S)2}}{(1 + \rho_i s_i^{(S)})^2} \sum_{i=1}^L \ln(2d_i n_i^{(D)})} \leq \\ & \prod_{i=1}^L (1 + \rho_i s_i^{(D)}) \sqrt{\sum_{i=1}^L \frac{\rho_i^2 b_i^{(D)2}}{(1 + \rho_i s_i^{(D)})^2} \sum_{i=1}^L \ln(2d_i n_i^{(D)})}, \end{aligned} \quad (35)$$

where Eq. (35) verifies our conjecture.

**Remark 5:** Our Conjecture 4 is a by-product of Theorem 1. Since the DenseNet is with the densest concatenation shortcuts, following our analysis and construction, the DenseNet will have a worse generalization bound than the network with any other shortcut topology. One thing we would like to underscore is that the bound derived in Eq. (24) for S3-Net( $\oplus$ ) is a manually-crafted loose bound, as we purposely concatenate the compact matrices with zero matrices, resulting in the amplified complexity of the hypothesis space. However, it is straightforward because our goal is to show that the generalization bound of the S3-Net( $\oplus$ ) is tighter than that of the DenseNet. In addition, we would like to mention that our conclusion is drawn on margin-based multi-class generalization bound. It is valuable to explore more theoretical analysis based on different perspectives to see if the same result can be made.

**Other Generalization Bounds:** In recent years, [50] and [51] have demonstrated generalization bounds of chain-like neural networks from different perspectives in terms of the depth  $L$  and the width  $p$  (defined as the maximum number of neurons in each layer) and norms of weight matrices in each layer. The exponential bound on  $L$  in [50] was derived by directly estimating Rademacher complexity, while the bound in [51] utilized PAC-Bayesian approach to obtain a bound that is rigorously more loose than that in [36]. These results are summarized in Table III.

TABLE III

THE EXISTING BOUNDS FROM OTHER PERSPECTIVES FOR CHAIN-LIKE NEURAL NETWORKS. WE USE  $B_{l,2}$  AND  $B_{l,F}$  TO DENOTE THE UPPER BOUNDS OF SPECTRAL NORM AND FROBENIUS NORM IN  $l^{th}$  LAYER.

THE  $m$  IS THE SIZE OF DATA.

Methods	Original Results
[50]	$\mathcal{O}\left(\frac{2^L \cdot \prod_{l=1}^L B_{l,F}}{\sqrt{m}}\right)$
[51]	$\mathcal{O}\left(\frac{\prod_{l=1}^L B_{l,2} \cdot \log(Lp)}{\gamma \sqrt{m}} (L^2 p \sum_{l=1}^L \frac{B_{l,F}^2}{B_{l,2}^2})^{1/2}\right)$

We apply the tactical tricks from [50] and [51] into the DenseNet and the resultant bounds are summarized in Table IV. The proof for them are put into Appendix B and C. Following the same spirit we used in Conjecture 4, in the sense of bounds in [50] and [51], we can also show that the generalization bounds of S3-Net( $\oplus$ ) are strictly lower than that of DenseNet.

TABLE IV

THE GENERALIZATION BOUNDS FOR DENSENET BY THE APPROACHES OF [50] AND [51].  $e$  IS THE NATURAL NUMBER. WE USE  $B_{l,2}$  AND  $B_{l,F}$  TO DENOTE THE UPPER BOUNDS OF SPECTRAL NORM AND FROBENIUS NORM IN  $l^{th}$  LAYER. THE  $m$  IS THE SIZE OF DATA.

Methods	Original Results
[50]	$\mathcal{O}\left(\frac{\prod_{l=1}^L (1+2B_{l,F})}{\sqrt{m}}\right)$
[51]	$\mathcal{O}\left(\frac{\prod_{l=1}^L (1+eB_{l,2}) \cdot \log(Lp)}{\gamma \sqrt{m}} (L^2 p \sum_{l=1}^L \frac{B_{l,F}^2}{(1+eB_{l,2})^2})^{1/2}\right)$

**Experiments:** Figure 1 shows the basic topology of S3-

Net. Here the shortcuts are used for concatenations. Suppose that  $y_l$  is the output of  $l^{th}$  module in the network of  $L$  layers, we characterize the workflow of the network architecture in the following way:

$$\begin{aligned} y_{l+1} &= H(y_l), \\ y_l &= H(y_0 \otimes y_1 \otimes y_2 \otimes \dots \otimes y_{l-1}), \end{aligned} \quad (36)$$

where  $\otimes$  is an aggregation operator. The operator module  $H(\cdot)$  can perform multiple operations including batch normalization [37], convolution, dropout [38] and so on, whose details are abstracted in our macro-structural view. Encouraged by the positive analysis for S3-Net, we are motivated to evaluate the performance of S3-Net in real-world applications. Different with intuitive design and neural architecture search, our approach has significantly better theoretical accountability, by which more trust can be gained from practitioners.

The above bound analysis motivates us to explore our S3-Net model numerically to see if it can truly deliver competitive results as promised.

**S3-Net( $\oplus$ ):** The S3-Net( $\oplus$ ) is implemented as a drop-in replacement for its counterpart DenseNet. That means the only difference between S3-Net( $\oplus$ ) and DenseNet is the topology of shortcut connections. We implemented our S3-Net( $\oplus$ ) in PyTorch Network. For the initialization strategy of S3-Net( $\oplus$ ), we followed the initialization strategy in Huang *et al.* The DenseNet utilized stage training, where the number of filters across the stages are doubled and the size of feature maps are reduced at the scale of 2. In Table V, we summarized our experimental results on the CIFAR-100. The parameter  $k$  is the feature growth rate used in DenseNet. Because S3-Net( $\oplus$ ) has the same structure with the DenseNet except the topology of shortcut connections, the parameter  $k$  also applies to S3-Net ( $\oplus$ ). The experimental results agree with what the generalization bound analysis predicted. It is seen that the S3-Net ( $\oplus$ ) achieves the competitive performance compared to the DenseNet. S3-Net ( $\oplus$ )-64-70 achieved the error rate of 22.76%, which is lower than that of DenseNet-24-100.

TABLE V  
THE COMPARISONS OF CLASSIFICATION PERFORMANCE AMONG VARIOUS ADVANCING MODELS ON CIFAR-100, WITH THE EMPHASIS ON DENSENET AND S3-NET( $\oplus$ ).

Network	Depth	#Params	error(%)
NIN + Dropout [10]	-	-	35.68
FractalNet with Dropout [20]	21	38.6M	35.34
ResNet (reported by [14])	110	1.7M	44.74
ResNet (Stochastic Depth) [39]	110	1.7M	37.80
ResNet (pre-activation) [40]	164	1.7M	35.58
DenseNet (k=12)	40	1.0M	27.55
DenseNet (k=12)	100	7.0M	23.79
DenseNet (k=24)	100	27.2M	23.42
S3-Net( $\oplus$ ) (k=12)	40	0.22M	29.80
S3-Net( $\oplus$ ) (k=24)	40	0.83M	26.46
S3-Net( $\oplus$ ) (k=40)	40	2.23M	24.16
S3-Net( $\oplus$ ) (k=64)	40	5.90M	23.30
S3-Net( $\oplus$ ) (k=64)	70	15.37M	22.76

We further summarize the results of Table V to evaluate the model efficiency, as shown in Figure 7, which highlights the high model efficiency enjoyed by S3-Net( $\oplus$ ), the red line (S3-Net( $\oplus$ )) is lying at the lower left side of the green line (DenseNet). Due to the much sparser shortcuts applied, S3-Net( $\oplus$ ) usually requires significantly less parameters in contrast to the DenseNet, especially when the growth number is small, but the performance of S3-Net( $\oplus$ ) is still superior than the DenseNet. S3-Net( $\oplus$ )-64-70 achieved error rate of 22.76%, which is lower than that of DenseNet-24-100.

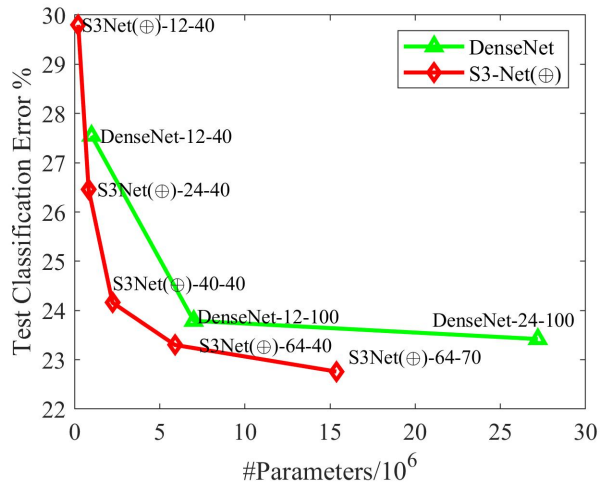


Fig. 7. The comparisons of model efficiency between S3-Net( $\oplus$ ) and Densenet on CIFAR-100 shows that S3-Net( $\oplus$ ) has better model efficiency and better performance.

## VI. CONCLUSION

In this study, we have demonstrated the power of skip connections in deep learning. We have firstly showed that a one-neuron-wide network of S3 topology is a universal approximator for any continuous univariate function. Then, we have presented a novel width-bounded universal approximator based on the S3-topology and the Kolmogorov-Arnold representation theorem, which adds a new member in the family of width-bounded universal approximators. After that we have presented a family of theoretically equivalent networks and corroborated the network equivalency with the experiments on CIFAR-10. Furthermore, we have showed the impact of concatenation shortcuts on the generalization bound of deep networks. As an immediate result, it is shown that the generalization bounds of S3-Net( $\oplus$ ) are tighter than those of DenseNet. Experimental results suggest that the S3-Net can achieve comparable or better learning performance than the densely connected networks. Future research directions can be put into the justification of network equivalency from the perspective of network optimization and exploring the utility of network equivalency in neural architecture search.

## REFERENCES

- [1] Y. LeCun, Y. Bengio and G. Hinton, "Deep learning", Nature, vol. 521, no. 7553, 2015.

- [2] F. Fan, W. Cong and G. Wang, "A new type of neurons for machine learning," *International journal for numerical methods in biomedical engineering*, vol. 34, no. 2, e2920, 2018.
- [3] G. E. Dahl, D. Yu, L. Deng and A. Acero, "Context-dependent pretrained deep neural networks for large-vocabulary speech recognition", *IEEE Transactions on audio, speech, and language processing*, vol. 20, no. 1, 2012.
- [4] A. Kumar et al., "Ask me anything: Dynamic memory networks for natural language processing," In *ICML*, 2016.
- [5] H. Chen, Y. Zhang, M. K. Kalra and et al. "Low-dose CT with a residual encoder-decoder convolutional neural network", *IEEE transactions on medical imaging*, vol. 36, no. 12, 2017.
- [6] G. Wang, "A Perspective on Deep Imaging, *IEEE Access*, vol. 4, pp. 8914-8924, 2016.
- [7] M. Anthimopoulos, S. Christodoulidis, L. Ebner, A. Christe, S. Mougiakakou, "Lung pattern classification for interstitial lung diseases using a deep convolutional neural network", *IEEE Trans. Med. Imaging*, vol. 35, pp. 1207-1276, 2016.
- [8] H. Shan et al., "3-D Convolutional Encoder-Decoder Network for Low-Dose CT via Transfer Learning From a 2-D Trained Network, *IEEE Trans. Med. Imaging*, vol. 37, pp. 1522-1534, 2018.
- [9] A. Krizhevsky, I. Sutskever, G. Hinton, "Imagenet classification with deep convolutional neural networks", In *NeurIPS*, 2012.
- [10] M. Lin, Q. Chen, S. Yan, "Network in network", In *ICLR*, 2014.
- [11] C. Szegedy, V. Vanhoucke, S. Ioffe, J. Shlens, Z. Wojna, "Rethinking the inception architecture for computer", In *CVPR*, 2016.
- [12] K. Simonyan and A. Zisserman, "Very deep convolutional networks for large-scale image recognition", In *ICLR*, 2015.
- [13] K. He, X. Zhang, S. Ren and J. Sun, "Deep residual learning for image recognition," In *CVPR*, 2016.
- [14] G. Huang, Z. Liu, L. Van Der Maaten and K. Q. Weinberger, "Densely connected convolutional networks", In *CVPR*, 2017.
- [15] X. Chu, B. Zhang, H. Ma, R. Xu, J. Li and Q. Li, "Fast, accurate and lightweight super-resolution with neural architecture search", *arXiv preprint arXiv:1901.07261*, 2019.
- [16] B. Hariharan, P. Arbeláez, R. Girshick and J. Malik, "Hypercolumns for object segmentation and fine-grained localization", In *CVPR*, 2015
- [17] V. Badrinarayanan, A. Kendall and R. Cipolla, "Segnet: A deep convolutional encoder-decoder architecture for image segmentation", *arXiv preprint arXiv:1511.00561*, 2015.
- [18] Q. Yao, J. Xu, W. W. Tu and Z. Zhu, "Efficient neural architecture search via proximal iterations", In *AAAI*, 2020.
- [19] R. K. Srivastava, K. Greff and J. Schmidhuber, "Highway networks", *arXiv preprint arXiv:1505.00387*, 2015.
- [20] G. Larsson, M. Maire and G. Shakhnarovich, "Fractalnet: Ultra-deep neural networks without residuals", *arXiv preprint arXiv:1605.07648*, 2016.
- [21] K. Funahashi, "On the approximate realization of continuous mappings by neural networks", *Neural networks*, vol. 2, pp. 183-192, 1989.
- [22] K. Hornik and M. Stinchcombe and H. White, "Multilayer feed-forward networks are universal approximators", *Neural networks*, vol. 2, pp.359-366, 1989.
- [23] L. Szymanski and B. McCane, "Deep networks are effective encoders of periodicity", *IEEE transactions on neural networks and learning systems*, vol. 25, pp. 1816-1827, 2014.
- [24] D. Rolnick and M. Tegmark, "The power of deeper networks for expressing natural functions", In *ICLR*, 2018.
- [25] N. Cohen, O. Sharir, and A. Shashua, "The power of deeper networks for expressing natural functions", In *COLT*, 2016.
- [26] H. N. Mhaskar and T. Poggio, "Deep vs. shallow networks: An approximation theory perspective", *Analysis and Applications*, vol. 14, pp. 829-848, 2016.
- [27] R. Eldan and O. Shamir, "The power of depth for feedforward neural networks", In *COLT*, 2016.
- [28] S. Liang and R. Srikant, "Why deep neural networks for function approximation?", In *ICLR*, 2017.
- [29] A. N. Kolmogorov, "On the representation of continuous functions of several variables by superpositions of continuous functions of a smaller number of variables", *Proceedings of the USSR Academy of Sciences*, vol. 108, pp. 179-182, 1956.
- [30] Z. Lu, H. Pu, F. Wang, Z. Hu and L. Wang, "The expressive power of neural networks: A view from the width", In *NeurIPS*, 2017.
- [31] F. Fan, J. Xiong and G. Wang, "Universal approximation with quadratic deep networks", *Neural Networks*, vol. 124, pp. 383-392, 2020.
- [32] H. Lin and S. Jegelka, "ResNet with one-neuron hidden layers is a Universal Approximator", In *NeurIPS*, 2018.
- [33] A. Veit and M. J. Wilber and S. Belongie, "Residual networks behave like ensembles of relatively shallow networks", In *NeurIPS*, 2016.
- [34] F. He, T. Liu and D. Tao, "Why resnet works? residuals generalize", *IEEE Transactions on Neural Networks and Learning Systems*, 2019.
- [35] L. Zhu, R. Deng, M. Maire, Z. Deng, G. Mori and P. Tan, "Sparsely Aggregated Convolutional Networks", In *ECCV*, 2018.
- [36] P. L. Bartlett, D. J. Foster and M. J. Telgarsky, "Spectrally-normalized margin bounds for neural networks", In *NeurIPS*, 2017.
- [37] S. Ioffe, and C. Szegedy, "Batch normalization: Accelerating deep network training by reducing internal covariate shift", *arXiv preprint arXiv:1502.03167*, 2015.
- [38] N. Srivastava, G. Hinton and A. Krizhevsky and I. Sutskever and R. Salakhutdinov, "Dropout: a simple way to prevent neural networks from overfitting", *The Journal of Machine Learning Research*, vol. 15, pp. 1929-1958, 2014.
- [39] G. Huang, Y. Sun, Z. Liu, D. Sedra and K. Q. Weinberger, "Deep networks with stochastic depth", In *ECCV*, 2014.
- [40] K. He, X. Zhang, S. Ren and J. Sun, "Identity mappings in deep residual networks", In *ECCV*, 2014.
- [41] H. Jin, Q. Song and X. Hu, "Auto-keras: An efficient neural architecture search system", In *KDD*, 2019.
- [42] S. Sabour, N. Frosst and G. E. Hinton, "Dynamic routing between capsules", In *NeurIPS*, 2017.
- [43] I. Goodfellow, D. Warde-Farley, M. Mirza, A. Courville and Y. Bengio, "Maxout networks", In *NeurIPS*, 2013.
- [44] M. F. Stollenga, J. Masci, F. Gomez and J. Schmidhuber, "Deep networks with internal selective attention through feedback connections", In *NeurIPS*, 2014.
- [45] M. Courbariaux, Y. Bengio and J. P. David, "Binaryconnect: Training deep neural networks with binary weights during propagations", In *NeurIPS*, 2015.
- [46] E Kang, H. J. Koo, D. H. Yang, J. B. Seo and JC Ye, "Cycle-consistent adversarial denoising network for multiphase coronary CT angiography", *Medical Physics*, vol. 46, pp. 550-562, 2019.
- [47] C You, G. Li, Y. Zhang, X. Zhang, H. Shan et al., "CT super-resolution GAN constrained by the identical, residual, and cycle learning ensemble (GAN-CIRCLE)", *IEEE Transactions on Medical Imaging*, vol. 39, pp. 188-203, 2019.
- [48] T. Liu, M. Chen, M. Zhou, S. S. Du, E. Zhou and T. Zhao, "Towards Understanding the Importance of Shortcut Connections in Residual Networks", In *NeurIPS*, 2019.
- [49] K. C. Das and P. Kumar, "Some new bounds on the spectral radius of graphs", *Discrete Mathematics*, vol. 281, pp. 149-161, 2004.
- [50] B. Neyshabur, R. Tomioka and N. Srebro, "Norm-based capacity control in neural networks", In *COLT*, 2015.
- [51] B. Neyshabur, R. Tomioka and N. Srebro, "A pac-bayesian approach to spectrally-normalized margin bounds for neural networks", In *ICLR*, 2018.
- [52] P. L. Bartlett, O. Bousquet and S. Mendelson, "Localized rademacher complexities", In *COLT*, 2018.